Published OnlineFirst September 4, 2019; DOI: 10.1158/2326-6066.CIR-19-0168

Research Article

Cancer Immunology Research

The Atypical Receptor CCRL2 Is Essential for Lung Cancer Immune Surveillance

Annalisa Del Prete[1,2], Francesca Sozio[1,2], Tiziana Schioppa[1,2], Andrea Ponzetta[2], William Vermi[1], Stefano Calza[1,3], Mattia Bugatti[1], Valentina Salvi[1], Giovanni Bernardini[4,5], Federica Benvenuti[6], Annunciata Vecchi[2], Barbara Bottazzi[2], Alberto Mantovani[2,7,8], and Silvano Sozzani[1]

Abstract

CCRL2 is a nonsignaling seven-transmembrane domain receptor. CCRL2 binds chemerin, a protein that promotes chemotaxis of leukocytes, including macrophages and natural killer (NK) cells. In addition, CCRL2 controls the inflammatory response in different pathologic settings, such as hypersensitivity, inflammatory arthritis, and experimental autoimmune encephalitis. Here, we investigated the role of CCRL2 in the regulation of lung cancer–related inflammation. The genetic deletion of *Ccrl2* promoted tumor progression in urethane-induced and in $Kras^{G12D/+}/p53^{LoxP}$ lung tumor mouse models. Similarly, a *Kras*-mutant lung tumor displayed enhanced growth in *Ccrl2*-deficient mice. This phenotype was associated with a reduced inflammatory infiltrate characterized by the impaired recruitment of several leukocyte populations including NK cells. Bone marrow chimeras showed that CCRL2 expression by the nonhematopoietic cell compartment was responsible for the increased tumor formation observed in *Kras*-mutant *Ccrl2*-deficient mice. In human and mouse lungs, CCRL2 was expressed by a fraction of $CD31^+$ endothelial cells, where it could control NK infiltration. Elevated CCRL2 expression in biopsies from human lung adenocarcinoma positively correlated with clinical outcome. These results provide evidence for a crucial role of CCRL2 in shaping an anti–lung tumor immune response.

Introduction

Lung cancer is the leading cause of cancer-related deaths worldwide, with non–small cell lung carcinoma (NSCLC) being approximately 85% of all lung cancers (1, 2). Lung adenocarcinoma (LUAD) and squamous cell carcinoma (LUSC) are the most common NSCLC histologic subsets (3). NSCLC subtypes are associated with several genetic alterations, such as activating mutations of *EGFR* or *KRAS* and loss-of-function mutations, like *TP53* (4). Growing evidence shows that in addition to the intrinsic properties of cancer cells, the tumor microenvironment (TME) plays a relevant role in the definition of tumor phenotype (5). Indeed, cancer-related inflammation is considered a key aspect of tumor growth and dissemination (6). Chemokines and related chemotactic factors are responsible for leukocyte tumor infiltration and control several aspects of tumor biology, including angiogenesis, cancer cell proliferation, and migration (7, 8). In tumors, chemokine expression is often dysregulated by cancer-associated genetic alterations (6).

Chemotactic factors bind seven-transmembrane G protein–coupled receptors and promote directional cell migration through the induction of a cascade of intracellular signaling events, such as activation of phospholypase C, calcium fluxes, and PI3Kγ. Chemotactic proteins also bind a subset of receptors referred to as atypical chemokine receptors (ACKR), which lack chemotactic activity and are believed to control inflammation through their ligand scavenging functions (9, 10). ACKRs play a role in inflammation and tumor biology, with the ability to either promote or limit tumor growth and dissemination (10, 11).

CCRL2 is a 7-transmembrane protein, closely related to the chemokine receptors (e.g., CCR1, CCR2, CCR3, and CCR5) that shares many characteristics with ACKRs, including the lack of certain consensus sequences and the inability to induce functional responses (9, 12). CCRL2 is expressed by a large variety of leukocyte subsets and barrier cells, including activated monocyte/macrophages, neutrophils, dendritic cells (DC), lymphocytes, mast cells, $CD34^+$ precursor cells, vascular and lymphatic endothelium, and some epithelial cells (13–19). CCRL2 binds chemerin, a nonchemokine chemotactic protein (16), and unlike other ACKRs, it does not bind chemokines and is devoid of ligand scavenging functions (20, 21). Rather, CCRL2 functions as a chemerin-presenting molecule on the surface of endothelial cells (14, 15) and in leukocytes, it can regulate the function of chemokine receptors, such as CXCR2 (18). Through these functions, CCRL2 was shown to tune the inflammatory response in different pathologic settings, such as hypersensitivity,

[1]Department of Molecular and Translational Medicine, University of Brescia, Brescia, Italy. [2]IRCCS Humanitas Clinical and Research Center, Rozzano, Italy. [3]Department of Medical Epidemiology and Biostatistics, Karolinska Institutet, Stockholm, Sweden. [4]Department of Molecular Medicine, Sapienza University of Rome, Laboratory Affiliated to Institute Pasteur-Italia, Rome, Italy. [5]IRCCS Neuromed, Pozzilli (IS), Italy. [6]International Centre for Genetic Engineering and Biotechnology, Trieste, Italy. [7]Humanitas University, Rozzano-Milano, Italy. [8]The William Harvey Research Institute, Queen Mary University of London, London, United Kingdom.

Note: Supplementary data for this article are available at Cancer Immunology Research Online (http://cancerimmunolres.aacrjournals.org/).

Corresponding Author: Silvano Sozzani, Department of Molecular and Translational Medicine, University of Brescia, Viale Europa 11, Brescia 25123, Italy. Phone: 3903-0371-7282; Fax: 3903-0371-7747; E-mail: silvano.sozzani@unibs.it

Cancer Immunol Res 2019;XX:XX–XX

doi: 10.1158/2326-6066.CIR-19-0168

Published OnlineFirst September 4, 2019; DOI: 10.1158/2326-6066.CIR-19-0168

inflammatory arthritis, and experimental autoimmune encephalitis (16–19).

The current study was performed to investigate the possible role of CCRL2 in the regulation of host defence in the TME. To test this hypothesis, we used models of lung cancer with molecular and histopathologic similarities with human *Kras*-driven lung carcinomas, such as LUAD; specifically, we used the genetic mouse *Kras*$^{G12D/+}$; *p53*^{LoxP} (TK) lung tumor model, the urethane chemically induced mouse lung tumor model, and the transplantable lung tumor LG1233 cell lines implanted into C57BL/6J mice. The results here reported a crucial role of CCRL2 in the orchestration of immune responses in the control of lung tumor development and progression.

Materials and Methods

Animals

Procedures involving animal handling and care conformed to protocols approved by the Humanitas Clinical and Research Center (Rozzano, Milan, Italy) in compliance with national (D.L. N.116, G.U., suppl. 40, 18-2-1992 and N. 26, G.U. March 4, 2014) and international law and policies (EEC Council Directive 2010/63/EU, OJ L 276/33, 22-09-2010; National Institutes of Health Guide for the Care and Use of Laboratory Animals, U.S. National Research Council, 2011). The study was approved by the Italian Ministry of Health (approval number 35/2013-B, issued on February 7, 2013, and number 165/2017-PR, issued on February 20, 2017). All efforts were made to minimize the number of animals used and their suffering.

B6.129P2-*Trp53*^{tm1Brn}/J (*p53*^{LoxP}) and *Kras*^{tm4Tyj}/J (*Kras*$^{LSL-G12D}$) were obtained from The Jackson Laboratory (cod 008462 and 008179, respectively) and initially crossed to obtain *p53*^{LoxP}/*Kras*$^{G12D/+}$. *p53*^{LoxP}/*Kras*$^{G12D/+}$ mice were then crossed with *Ccrl2* knockout (KO) to obtain the two lines *p53*^{LoxP}/*Kras*$^{G12D/+}$/*Ccrl2*$^{+/+}$ [TK-*Ccrl2* wild type (WT)] and *p53*^{LoxP}/*Kras*$^{G12D/+}$/*Ccrl2*$^{-/-}$ (TK-*Ccrl2* KO). Mice genotyping was performed by PCR.

All mice used [WT and *Ccrl2* KO, (19); TK-*Ccrl2* WT and TK-*Ccrl2* KO] were on C57BL/6J genetic background (over 10 generation backcrossed); all colonies were bred in Charles River Laboratories and housed in the specific pathogen–free animal facility of Humanitas Clinical and Research Center.

Urethane-induced lung carcinogenesis model

Six- to 7-week-old WT and *Ccrl2* KO male mice were intraperitoneally injected with urethane (1 mg per g body weight in 200 μL; Sigma) dissolved in saline weekly for 10 weeks as described previously (22) and fed with antioxidant free laboratory diet chow (Teklad Global 19% Protein Extruded Rodent Diet, ENVIGO). Mice were sacrificed 30 weeks after the first urethane injection and lungs, spleen, blood, and bone marrow were harvested. Briefly, lungs were collected upon intracardiac perfusion with cold PBS. Right lung lobes were mechanically cut into small pieces and then enzymatically treated with collagenase D (IV type, *Clostridium histolyticum*, Sigma) 1 mg/mL and DNase I (from bovine pancreas grade 2, Roche) 0.02 mg/mL at 37°C for 30 minutes. Enzymatic reaction was stopped by EDTA (Sigma), and single-cell suspension was filtered through a 70-μm cell strainer and stained for cytofluorimetric analysis. Left lung lobes were formalin fixed for 24 hours, dehydrated, and paraffin embedded for histologic analysis. Spleens were smashed using the plunger of a syringe through 70-μm cell strainer to obtain a single-cell suspension; bone marrow cells were obtained by flushing with cold PBS of the cavity of freshly dissected femurs filtered through 70-μm cell strainer and blood was collected from retro orbital sinus. All single-cell suspensions were then stained for cytofluorimetric analysis after red blood cell lysis with ice-cold ACK Lysing Buffer for 5 minutes (Lonza).

Kras/p53-driven lung cancer model

TK-*Ccrl2* WT and TK-*Ccrl2* KO, at 8 weeks of age, were intranasally inoculated with 2.5×10^7 infectious particles of replication-deficient adenoviral vector (in 50 μL DMEM with 10 mmol/L $CaCl_2$) with cytomegalovirus promoter driving the expression of the Cre recombinase protein (Ad5CMVCre) to induce sporadic mutations and lung tumor development as described previously (23). Mice were sacrificed 10 weeks after the adenovirus inoculation and lungs, spleen, and bone marrow were collected and treated as described for urethane model. Furthermore, the accessory lung lobe was immediately frozen at −80°C and used for real-time PCR.

Flow cytometry/intracellular staining

Single-cell suspensions from bone marrow, blood, spleen, and lung were stained with the following antibodies: CD45-BV605 (clone: 30-F11) or –VioGreen (clone: REA737); NK1.1-PECF594 or -APC (clone: PK136); CD11b-APCCy7 or PE-Vio770 (clone: M1/70); CD27-PECy7 (clone: LG.7F9); CD4-FITC or –PE-Vio770 or -AF700 (clone RM 4-5); CD8-BV570 or -VioBlue (clone 53-6.7); Granzyme B-PEeF610 (clone: NGZB); Perforin-PE (clone: eBioOMAK-D); IFNγ-Alexa700 (clone: XMG1.2); CD107a-BV786 (clone: H4A3); Eomes AF488 (clone:Dan 11 mag); CD49b-APC (clone: DX5); CD49a-BV711 (clone: Ha31/8); TCRβ-PerCp (clone: H57-597); TCRγδ-BV421 (clone: GL3); Ly6G-FITC (clone1A8); Ly6C-PE (clone REA796); CD19-VioBlue (clone REA749); F4/80-PercP-Vio770 (clone REA126); CD45RA-APC-Vio770 or PE-Vio770 (clone T6D11); MHCII-FITC or –VioBlue (clone REA564); CCRL2-PE (clone BZ2E3); SiglecH-APC (clone 551.3D3); CD11c-PercP-Cy5.5 (clone: REA 754); CD3-PE (clone 145-2C11) or PercP-Cy5.5 (clone17A2); SiglecF-FITC (clone: REA 798); CD31-APC (clone: MEC 13.3); EpCam-VioBlue (clone REA977); CD127-BV786 (clone: 5B/199) from BD Biosciences, eBioscience, BioLegend, Miltenyi Biotec, and Invitrogen. Subsequently, cell viability was determined by Aqua LIVE/Dead-405 nm (L34965) or LIVE/Dead-633 nm (L10120) or LIVE/Dead-488 nm (L34969) staining according to the manufacturer's instructions (Invitrogen); negative cells were considered viable. A Foxp3/Transcription Factor Staining Buffer Set (eBioscience) was used for intracellular staining of granzyme B, perforin, IFNγ, and CD107a according to the manufacturer's instructions. Cells were analyzed on an LSR Fortessa (BD Biosciences) or MACSQuant (Miltenyi) and analyzed with FlowJo software (Treestar).

Lung histology and IHC

Histology was performed on five (urethane-induced model) or seven (*Kras/p53*-driven model) longitudinal serial sections (150 μm apart, 4 μm in thickness) from each left lung, stained with hematoxylin and eosin (H&E), and scanned by VS120 Dot-Slide BX61 virtual slide microscope (Olympus Optical). The total number and area of lung lesions were obtained by manually tracing the perimeter of lesions using the Image Pro-Premiere software (Media Cybernetics).

Published OnlineFirst September 4, 2019; DOI: 10.1158/2326-6066.CIR-19-0168

IHC

NKp46 IHC staining was performed on tissue slides (4 μm in thickness) that were rehydrated in alcohol (100%, 90%, 70%, and 50%; 1 minute each step) and placed in citrate buffer 1 mol/L (for 15 minutes in a Whirlpool microwave) for antigen retrieval. Endogenous peroxidase activity was quenched with 3% H_2O_2 for 20 minutes and unspecific binding sites were blocked for 30 minutes with Rodent Block M (Biocare Medical). Samples were then incubated 1 hour with Goat Anti-Mouse NKp46 (AF2225 R&D Systems) and detected by Goat on Rodent Polymer Kit (Biocare), followed by DAB Chromogen Kit (Biocare). Matched IgG was used as a negative control. For Ly6G immunostaining, Rat Anti-Mouse Ly6G (BD Biosciences) was used. To localize CCRL2-positive cells in the lungs, tissues were analyzed with RNAscope assay (Advanced Cell Diagnostics) using RNAscope 2.5 HD Assay-RED Kit and Mm-Ccrl2-No-Xhs probes. Sections from fixed mouse tissue blocks were treated following the manufacturer's instructions. Briefly, freshly cut 3-μm sections were deparaffinized in xylene and treated with the peroxidase block solution for 10 minutes at room temperature followed by the retrieval solution for 15 minutes at 98°C and by protease plus at 40°C for 30 minutes. Control probes included positive control Mm-Polr2a and negative control dapB. The hybridization was performed for 2 hours at 40°C. The signal was revealed using RNAscope 2.5 HD Detection Reagent and FAST RED.

LG1233 cells

The LUAD cell line LG1233 was derived from lung tumors of C57BL/6 KP mice (K-rasLSL-G12D/þ;p53fl/fl mice) and was kindly provided by Dr. Tyler Jacks (Massachusetts Institute of Technology, Cambridge, MA) in July 2015. LG1233 was not authenticated. The cell line was maintained in DMEM supplemented with 10% FBS and gentamicin (50 μg/mL) and routinely tested for *Mycoplasma* contamination. LG1233 cells were expanded to passage 3 and stored in aliquots in liquid nitrogen; to induce tumors, cells were cultured less than five passages (24, 25). Cells were harvested and wash three times with PBS and then 1×10^5 cells in 100 μL of PBS were injected intravenously in the caudal vein. Lungs were collected 13 days after engraftment and used for histology and FACS analysis.

Specific depletion or blocking experiments

The anti-NK1.1 depletion experiment was performed in *Kras/p53*–driven lung cancer model, while the CCRL2 blocking in the LG1233 cell line lung metastasis model. Mice were treated at day −1 intraperitoneally with 100 μg of anti-NK1.1 (clone PK136) or isotype control (clone C1.18.4) and anti-CCRL2, generated in the laboratory (19), or isotype control (clone MPC-11; all from Bio X Cell). Mice were then treated with 100 μg/100 μL PBS once (anti-NK1.1) or three times (anti-CCRL2) a week for the entire duration of the experiment.

Bone marrow transplantation

TK-*Ccrl2* WT and KO mice were lethally irradiated with a total dose of 9 Gy using a RADGIL 2, X-ray irradiator (Gilardoni). Then, 2 hours later, mice were injected in the retro-orbital plexus with 5×10^6 nucleated bone marrow cells obtained by flushing of the cavity of freshly dissected femurs from TK-*Ccrl2* WT or KO mice. Eight weeks after bone marrow transplantation, mice were intranasally inoculated with 2.5×10^7 infectious particles of Ad5CMVCre. After 10 weeks, mice were sacrificed then lungs were perfused, collected, and processed as described previously.

Transmigration assay

Vascular endothelial 1G11 cells were grown to confluence on 0.1% gelatin-coated transwell inserts in 24-well costar chambers (5 μm pore size; Corning). The endothelial cells were stimulated with IFNγ (50 ng/mL), TNFα (20 ng/mL), and LPS (100 ng/mL) in DMEM medium containing 0.2% BSA (migration medium) for 18 hours. For the transmigration assay, splenic natural killer (NK) cells purified by using NK Negative Isolation Kit according to the manufacturer's instructions (cat. no. 130-115-818, Miltenyi Biotec), according to the manufacturer's instructions. Purified NK cells (3×10^5 in 100 μL migration medium) were placed in the upper chamber and 600 μL of chemerin (200 nmol/L) or control medium was added to the lower chamber. NK cells were allowed to migrate at 37°C in a 5% CO_2 atmosphere for 4 hours. NK-cell migration was evaluated as the percentage of $CD3^-NK1.1^+$ recovered in the lower compartment relative to input by flow cytometry. When indicated, 1G11 vascular endothelial cells were pretreated (1 hour at 37°C) with anti-CCRL2 mAb (10 μg/mL) or isotype control mAb, and washed before NK transmigration.

Migration assay

Chemotaxis assays in response to CXCL12, CXCL10, CCL5, CX3CL1 (200 ng/mL, Peprotech), and chemerin (100 nmol/L, R&D Systems) were performed in 5-μm pore Transwell insert. Spleen cells (5×10^5) from individual animals were loaded in the upper well. After 90 minutes, the contents of the lower chemotaxis well, following Transwell insert removal, were centrifuged at $300 \times g$ for 10 minutes. After Fc blocking with CD16/32 antibody (clone 2.4G2), the cells were incubated with an antibody mixture appropriate to evaluate NK-cell subsets. Cell migration was assessed by FACS and calculated as percentage of input cells for each NK subset.

Cytotoxicity assay

Splenic NK-cell cytotoxicity was determined after 24 hours of incubation in the presence of IL12 (50 ng/mL) and IL15 (50 ng/mL), against the YAC-1 target cells labeled with 1 μmol/L of CFSE. Effector cells (E) were mixed with 50,000 target cells (T) at E/T ratios ranging from 1/1 to 50/1. After 4 hours of incubation at 37°C in 96-well plate, the percentage of killed target cells was evaluated by FACS as CFSE-positive cells from the Live DEAD-405 nm positive cells.

Gene expression (qPCR)

FACS-sorted lung and splenic NK cells from TK-*Ccrl2* WT and KO mice were analyzed for mRNA expression of the indicated genes by qPCR. RNA was extracted with the RNeasy Kit (Qiagen) according to the manufacturer's instructions and quantified by NanoDrop (Thermo Fisher Scientific). After RNA purification, reverse transcription was performed using random hexamers and MMLV RT (Thermo Fisher Scientific). Gene-specific primers used were as follows: *Cxcl10* (forward: 5′-cgtcatttttctgcctcatcctg-3′, reverse: 5′-ccgtcatcgatatggatgcagt-3′), *Cx3cl1* (forward: 5′-catccgctatcagctaaacca-3′, reverse: 5′-cagaagcgtctgtgctgtgt-3′), *Ccl5* (forward: 5′-ctcaccatcatcctcactgcag-3′, reverse: 5′-gagaggtaggcaaagcagcag-3′), *Rarres 2* (forward: 5′-ggagtgcacaatcaaaccaa-3′, reverse: 5′-ttttacccttggggtccatt-3′), *Cmklr1* (forward: 5′-ccatgtgcaagatcagcaac-3′,

Published OnlineFirst September 4, 2019; DOI: 10.1158/2326-6066.CIR-19-0168

reverse: 5′-gcaggaagacgctggtgta-3′), *Ccr5* (forward: 5′-gagcgtgactgatatctacctg-3′, reverse: 5′-cactcatttgcagcatagtgagc-3′), *Cxcr3* (forward: 5′-gctgctgtgctactgagtcagc-3′, reverse: 5′-actggacagcagcatccactgc-3′), *Cx3cr1* (forward: 5′-cttcatcaccgtcatcagcatc-3′, reverse: 5′-gactaatggtgacaccgtgctg-3′), *Ifnγ* (forward: 5′-atctggaggaactggcaaaa-3′, reverse: 5′-ttcaagacttcaaagagtctgaggta-3′), *Gzme* (forward: 5′-cccaaagaccaaacgtgcttcc-3′, reverse: 5′-aagcacgtcgaggtgaaccatc-3′), *Prf1* (forward: 5′-cgacacagtagagtgtcgcatg-3′, reverse: 5′-cctgtggtaagcatgctctgtg-3′), *Pdcd1* (forward: 5′-tgcagttgagctggcaat-3′, reverse: 5′-ggctgggtagaaggtgagg-3′), *Cd274* (forward: 5′-aaatcgtggtccccaagc-3′, reverse: 5′-aatatcctcatgttttgggaactatc-3′), *Pdcd1lg2* (forward: 5′-gcatgttctggaatgctcac-3′, reverse: 5′-ctttgggttccatccgact-3′), *Lag3* (forward: 5′-cacctgtagcatccatctgc-3′, reverse: 5′-ccaggtaacccgaaggattt-3′), *Ikzf3* (forward: 5′-ccagccaatgaagacgaag-3′, reverse: 5′-ccggcttcataatgttctcat-3′), *Nfil3* (forward: 5′-ctttctttttcccctcacg-3′, reverse: 5′-caggagcctttcatgggtta-3′), *Eomes* (forward: 5′-ggcctaccaaaacacggata-3′, reverse: 5′-gacctccagggacaatctga-3′), *Tbx21* (forward: 5′-tcaaccagcaccagacagag-3′, reverse: 5′-atcctgtaatggcttgtggg-3′), *Id2* (forward: 5′-gacagaaccaggcgtcca-3′, reverse: 5′-agctcagaagggaattcagatg-3′), *Il2* (forward: 5′-gctgttgatggacctacagga-3′, reverse: 5′-ttcaattctgtggcctgctt-3′), *Il15* (forward: 5′-agcactgcctcttcatggtc-3′, reverse: 5′-ctgccatccatccagaactc-3′), *Il15ra* (forward: 5′-ggagtccaggccattcct-3′, reverse: 5′-cagcatgctcaatagatacgg-3′), *Il18* (forward: 5′-caaaccttccaaatcacttcct-3′, reverse: 5′-tccttgaagttgacgcaaga-3′) and *Rpl32* (forward: 5′-gctgccatctgttttacgg-3′, reverse: 5′-tgactggtgcctgatgaact-3′) used for normalization. The SsoAdvanced Universal SYBR Green Supermix (Bio-Rad Laboratories) for quantitative real-time PCR was used according to the manufacturer's instructions. Reactions were run in triplicates on a StepOne Plus Real-Time PCR System (Applied Biosystems) and the generated products analyzed by the StepOne Plus Software (Version 2.3, Applied Biosystems).

The Cancer Genome Atlas datasets

LUAD RNA-Seq data (recorded as gene-level counts) were downloaded from The Cancer Genome Atlas/Genomic Data Commons (TCGA/GDC; DbGaP Study Accession: phs 000178) using the "harmonized" set as count data using R/Bioconductor package-*TCGAbiolink*s (version 2.8.4). Paired data (Solid Tumor and Solid Normal) were modeled using weighted linear models accounting for variance-mean relationship after TMM normalization. In total, we considered 57 LUAD samples with matched Solid Normal Tissue and Solid Tumor Tissue. When considering only tumors, we analyzed a total of 513 LUAD samples. When used as a biomarker, CCRL2 expression was computed as $\log_2$ counts per million. Data were analyzed with R (version 3.51) and Bioconductor software.

Statistical analysis

Statistical analyses were performed by Student *t* test, Mann–Whitney test, as appropriate. Count data (number of lesions) were modeled using Poisson regressions. Counts were derived from multiple lung slices from the same mouse, and data were modeled using generalized linear mixed models to account for within sample correlation. Poisson regression might poorly fit data with a great number of zero counts (no lesions). To account for this, zero-inflated Poisson regression models were considered. Results were analyzed by using GraphPad PRISM 5.0 and R (version 3.51) software and expressed as mean ± SEM (*, $P < 0.05$; **, $P < 0.01$; ***, $P < 0.001$).

Results

Ccrl2 deficiency increased tumor burden in urethane-induced carcinogenesis

Urethane-induced tumors are known to recapitulate many aspects of human lung cancer including some gene mutations and histologic features (22). *Ccrl2* WT and *Ccrl2*-deficient mice were weekly administered intraperitoneally with urethane (1 mg/g) for a total of 10 doses, and sacrificed 30 weeks after the first injection, as described previously (22). This time point was selected on the basis of tumor incidence (around 90%) and number of lesions (22). Lung histologic analysis showed a significant increase of tumor multiplicity in *Ccrl2*-deficient mice compared with control animals (6.4 ± 0.5 vs. 4.8 ± 0.5; $P = 0.03$; Fig. 1A). The increased tumor burden was associated with the reduction of total inflammatory infiltrate, including interstitial perivascular and peribronchiolar lymphoid infiltrates and aggregates, as evaluated by the inflammatory score in histologic analysis (Fig. 1A). Characterization of the lung tumor microenvironment, performed by FACS analysis, revealed that *Ccrl2* deficiency was associated with a reduced frequency of some myeloid cell subsets (i.e., monocytes and macrophages), whereas the distribution of DCs and T and B lymphocytes was not affected (Fig. 1B). Also, neutrophils (polymorphonuclear, PMN), a leukocyte subset known to be associated with lung tumor growth (26) and to be regulated by CCRL2 (18), trended toward reduction in *Ccrl2*-deficient mice (Fig. 1B). The leukocyte subset that was most consistently reduced in the lungs of *Ccrl2*-deficient mice was NK cells. This reduction was documented both by FACS analysis (Fig. 1C; $P < 0.0001$) and by IHC in histologic sections using an anti-NKp46 antibody (Fig. 1D; $P < 0.05$). NK-cell frequency was impaired not only in the lung, but also in the spleen and in the blood compartments of tumor-bearing *Ccrl2*-deficient mice (Fig. 1C). Conversely, no difference was found in the number of NK cells in the bone marrow of *Ccrl2*-deficient mice (Fig. 1C). Of note, no difference in NK-cell distribution was observed between healthy WT and *Ccrl2*-deficient mice. Taken together, our results supported a protective role of CCRL2 in urethane-induced lung carcinogenesis through its ability to regulate the inflammatory tumor microenvironment.

Ccrl2 deficiency promoted tumor progression in a genetic model of Kras-mutated lung tumor

Because urethane-induced lung carcinogenesis is associated with *Kras* mutations (22), the role of CCRL2 in *Kras* mutation–dependent lung cancer was further investigated crossing $Kras^{G12D/+}$; $p53^{LoxP}$ (TK) with *Ccrl2*-deficient mice; carcinogenesis was induced by intranasal delivery of replication-deficient adenoviral vector with cytomegalovirus promoter driving the expression of the Cre recombinase protein (Ad5CMVCre), as described previously (23). The survival of TK-*Ccrl2*–deficient mice was dramatically reduced compared with TK-*Ccrl2* WT mice (median survival, 173.0 days vs. 137.5 days, respectively; $P < 0.0001$) with the lungs of TK-*Ccrl2*–deficient mice showing an increased number and larger size of tumor lesions compared with TK-*Ccrl2*-WT animals (Fig. 2A). Multiparametric flow cytometry of tumor microenvironment confirmed NK cells as the main cell population affected by *Ccrl2* deficiency, with $Ly6G^+$ neutrophils trending toward reduction both in the intratumoral and extratumoral areas (Supplementary Fig. S1A and S1B). A significant reduction of $CD3^-NK1.1^+$ cells was detected in the lung and in the spleen of

Published OnlineFirst September 4, 2019; DOI: 10.1158/2326-6066.CIR-19-0168

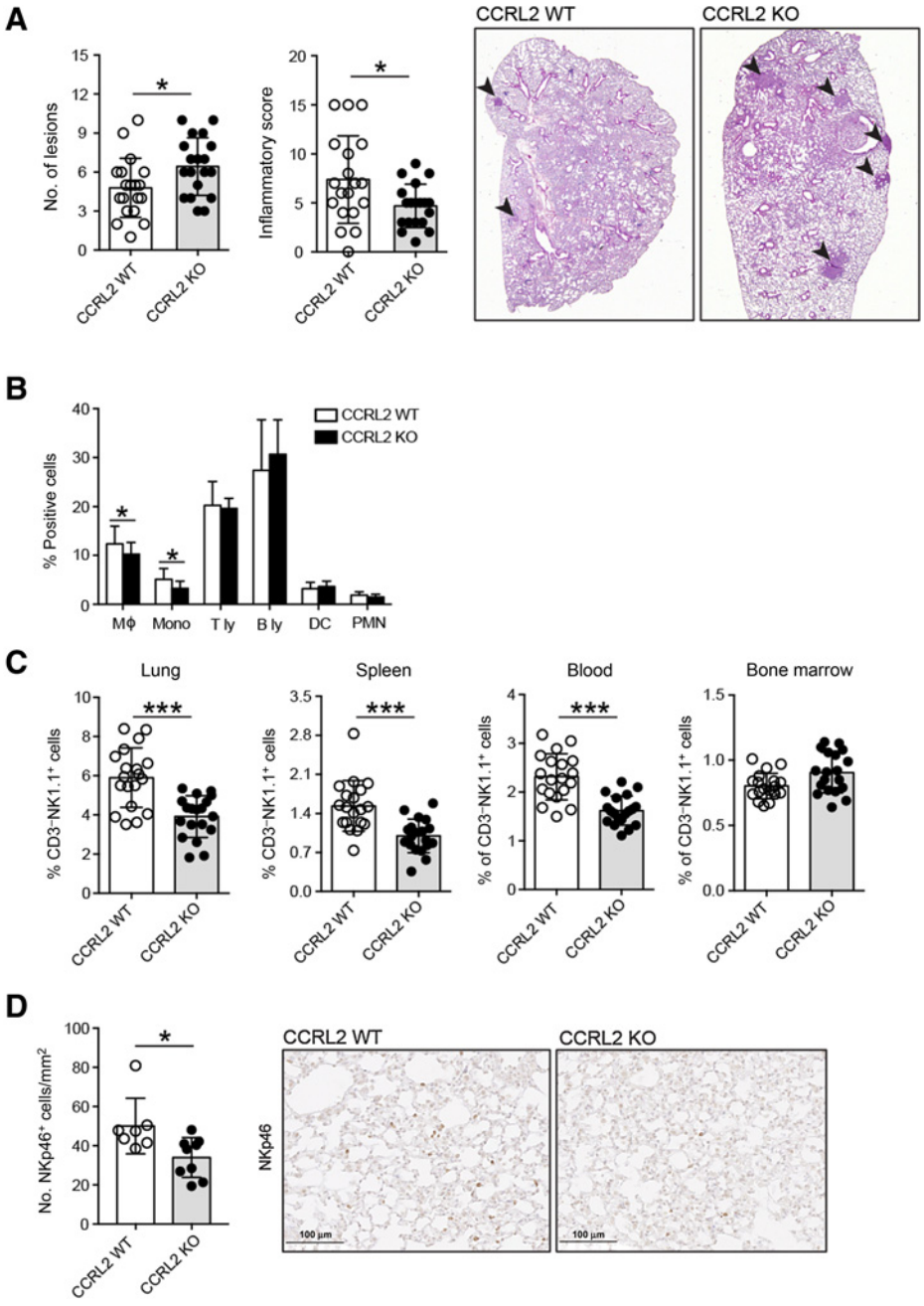

Figure 1.

Ccrl2 deficiency increased tumor burden in urethane-induced carcinogenesis. **A,** Number of neoplastic lesions and inflammatory score at the time of sacrifice (30 weeks after the first urethane injection) in the lungs of *Ccrl2* WT and *Ccrl2*-deficient (KO) mice. Evaluation was performed microscopically on histologic preparations of the lungs. Grading of inflammatory infiltrate: 0 = absence of lymphoid infiltrates/aggregates; 1 = 1–2 foci of interstitial perivascular/peribronchiolar lymphoid infiltrates/aggregates; 2 = 3–5 foci, 3 ≥ 5 foci. *, $P < 0.05$, *Ccrl2* WT ($n = 19$) versus *Ccrl2* KO ($n = 19$) by Mann–Whitney test. Data from one representative out of two independent experiments are shown and expressed as mean ± SEM. Representative H&E images of *Ccrl2* WT and CCRL *Ccrl2* KO lung sections showed the presence of neoplastic lesions (indicated with arrowheads). Objective magnification, ×12.5. **B,** Analysis of the inflammatory infiltrate by FACS. Single-cell suspensions were obtained by mechanical and enzymatic treatment of lungs, and the percentage of each leukocyte subpopulation was evaluated within the $CD45^+$ positive population. *, $P < 0.05$, *Ccrl2* WT ($n = 19$) versus *Ccrl2* KO ($n = 19$) by Student *t* test. Data from one representative out of two independent experiments are shown and expressed as mean ± SEM. B ly, B lymphocyte; Mo, monocyte; PMN, polymorphonuclear granulocyte; T ly, T lymphocyte. **C,** The percentage of $CD3^-NK1.1^+$ cells in the $CD45^+$ population was evaluated in lung, spleen, blood, and bone marrow of *Ccrl2* WT and *Ccrl2* KO tumor-bearing mice by FACS analysis. ***, $P < 0.001$, *Ccrl2* WT ($n = 19$) versus *Ccrl2* KO ($n = 19$) by Student *t* test. Data from one representative out of two independent experiments are shown and expressed as mean ± SEM. **D,** Histologic evaluation of $NKp46^+$ NK cells, quantified as the number of NKp46-positive cells (left) evaluated in four random ×10 microscopic fields selected throughout the lung parenchyma; right, representative sections. *, $P < 0.05$, *Ccrl2* WT ($n = 7$) versus *Ccrl2* KO ($n = 9$) by Mann–Whitney test. Data from one representative out of two independent experiments are shown and expressed as mean ± SEM.

Published OnlineFirst September 4, 2019; DOI: 10.1158/2326-6066.CIR-19-0168

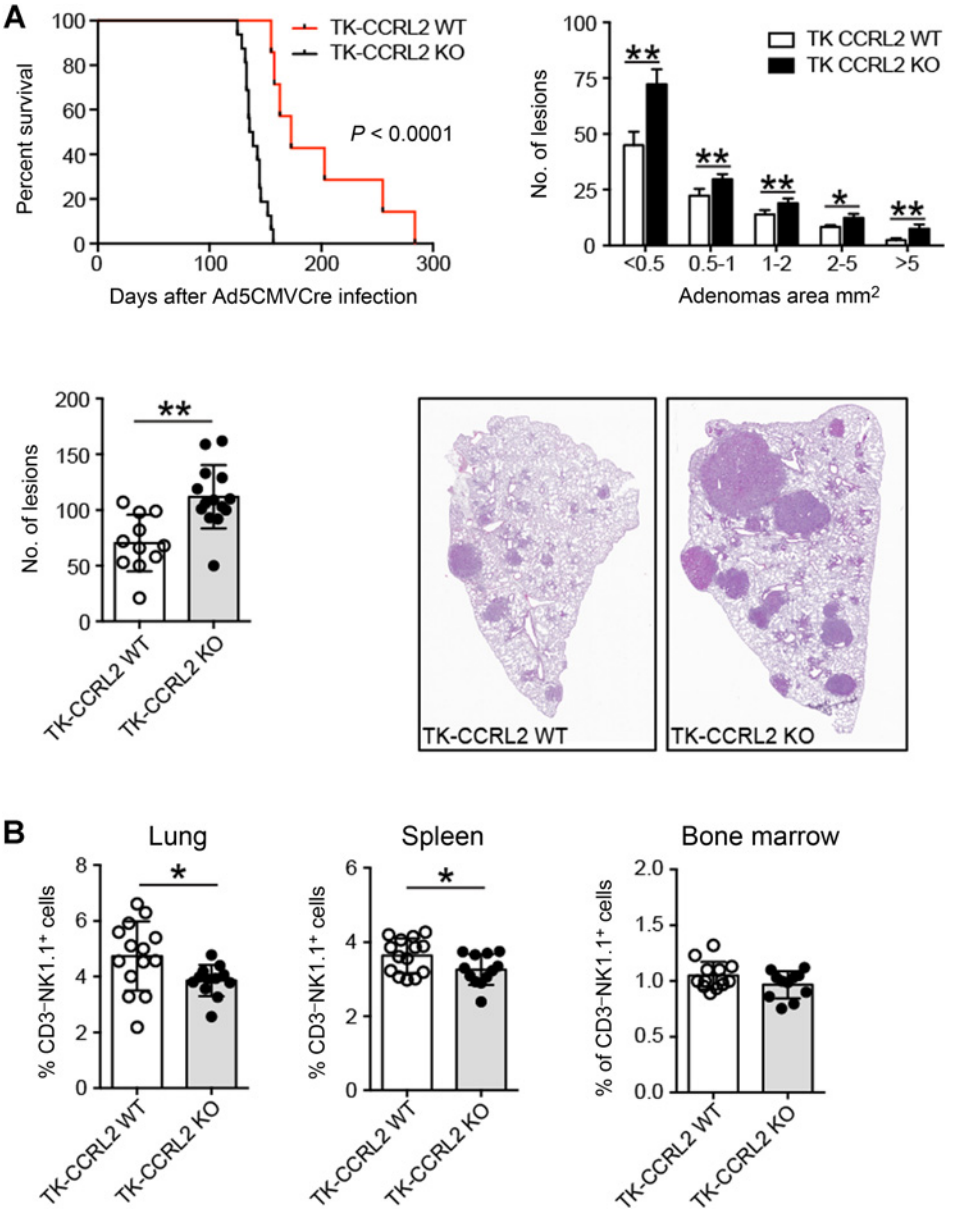

Figure 2.

Ccrl2 deficiency promoted tumor progression in $Kras^{G12D/+}$; $p53^{LoxP}$ (TK) mice. **A,** Top left, percentage of survival (median survival, TK-*Ccrl2* WT 173.0 days vs. TK-*Ccrl2* KO 137.5 days, respectively; $P < 0.0001$) after intranasal inoculation of 2.5×10^7 infectious particles of Ad5CMVCre recombinase. Top right and bottom left, the number (bottom left) and dimension (top right) of lesions 10 weeks after Ad5CMVCre infection. *, $P < 0.05$; **, $P < 0.01$, TK-*Ccrl2* WT ($n = 11$) versus TK-*Ccrl2* KO ($n = 14$) by Mann–Whitney test. Data from one representative out of four independent experiments are shown and expressed as mean ± SEM. Bottom right, representative histologic sections from TK-*Ccrl2* WT and TK-*Ccrl2* KO mice. Objective magnification ×10. **B,** The percentage of $CD3^-NK1.1^+$ cells in the $CD45^+$ cells evaluated in the lungs, spleens, and bone marrow, 10 weeks after Ad5CMVCre recombinase infection. *, $P < 0.05$, TK-*Ccrl2* WT ($n = 14$ lung and spleen, $n = 13$ bone marrow) versus TK-*Ccrl2* KO ($n = 12$ lung and spleen, $n = 11$ bone marrow) by Student *t* test. Data from one representative out of four independent experiments are shown and expressed as mean ± SEM.

TK-*Ccrl2*–deficient mice, whereas no difference was observed in the bone marrow (Fig. 2B). IHC performed on TK-*Ccrl2*–deficient mice confirmed the reduction of lung NK cells evaluated as $NKp46^+$ cells (Supplementary Fig. S2). Independently of their relative frequency, the distribution of NK cells was similar in TK-*Ccrl2* WT and KO mice, being mostly confined to the peritumoral areas (invasive margins), with very few $NKp46^+$ cells present within the tumor lesions (Supplementary Fig. S2).

NK-cell subsets were evaluated by the reciprocal expression of surface markers CD27 and CD11b, with $CD27^+CD11b^-$ cells being the most immature subset, double positive cells ($CD27^+CD11b^+$) at an intermediate stage of maturation, and $CD27^-CD11b^+$ cells the most mature subset (27). TK-*Ccrl2*–deficient mice had an altered distribution of NK-cell subsets both in the lung and spleen with a decreased frequency of the most mature $CD27^-CD11b^+$ population and increased frequency of $CD27^+CD11b^-$ NK cells (Fig. 3A). On the contrary, no difference was observed in NK-cell subset distribution in the bone marrow (Fig. 3A). To get more insights in the mechanisms responsible for the altered presence of NK cells in tissues, different strategies were pursued. First, the chemotactic ability of NK cells from TK-*Ccrl2*–deficient mice was evaluated in response to agonists of chemotactic receptors known to be preferentially expressed by NK cells at different maturation stages, namely CXCR4, CCR5, and CXCR3 for the most immature NK-cell subset ($CD27^+CD11b^-$) and CX3CR1 and CMKLR1 for the most mature NK-cell subset ($CD27^-CD11b^+$; ref. 28). NK-cell subsets purified from *Ccrl2*-deficient and WT mice revealed the expected migration profile that characterizes the cell maturation stage (Fig. 3B). However, the migration of *Ccrl2*-deficient mice-derived $CD27^-CD11b^+$ cells was reduced compared with their WT counterparts (Fig. 3B). Second, the expression of NK-cell chemotactic factors was

Published OnlineFirst September 4, 2019; DOI: 10.1158/2326-6066.CIR-19-0168

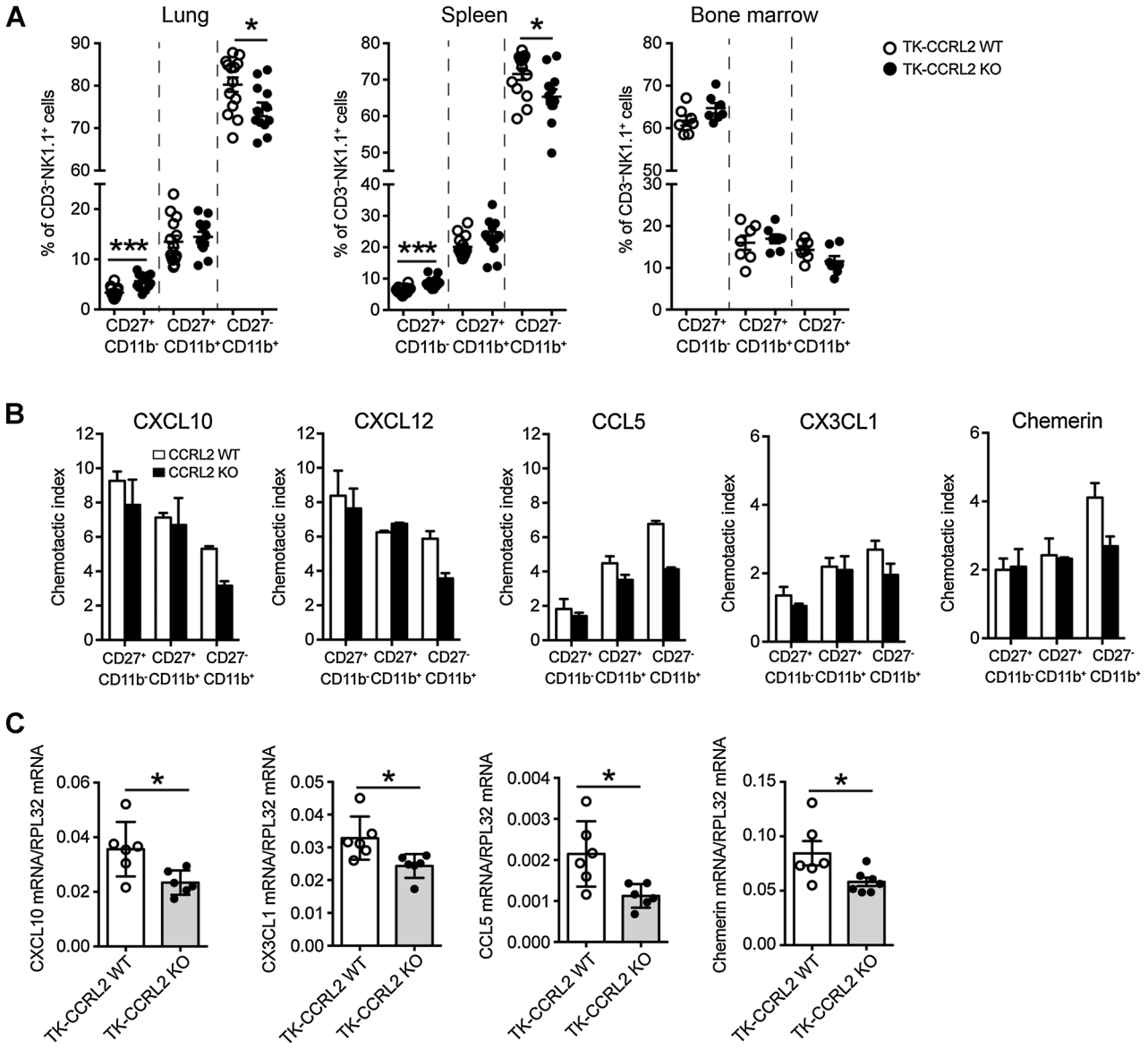

Figure 3.

Ccrl2 deficiency altered NK-cell subsets distribution and affected NK-cell tumor infiltration in tumor-bearing *Kras*$^{G12D/+}$;*p53*^{LoxP} (TK) mice. **A,** FACS analysis of the main NK subsets, CD27$^+$CD11b$^-$, CD27$^+$CD11b$^+$, and CD27$^-$CD11b$^+$, evaluated on CD3$^-$NK1.1$^+$ gated cells from lung, spleen, and bone marrow. *, $P < 0.05$; ***, $P < 0.001$, TK-*Ccrl2* WT ($n = 14$ lung and spleen, $n = 7$ bone marrow) versus TK-*Ccrl2* KO ($n = 12$ lung and spleen, $n = 7$ bone marrow) by Student *t* test. Data from two (lung and spleen) and one (bone marrow) independent experiments are shown and expressed as mean ± SEM. **B,** The chemotactic responses of splenic NK subsets CD27$^+$CD11b$^-$, CD27$^+$CD11b$^+$, and CD27$^-$CD11b$^+$ to CXCL12 (200 ng/mL), CXCL10 (200 ng/mL), CCL5 (200 ng/mL), CX3CL1 (200 ng/mL), and chemerin (100 nmol/L) after 90 minutes of migration was evaluated by FACS analysis on CD3$^-$NK1.1$^+$ gated cells from *Ccrl2* WT and KO spleen. TK-*Ccrl2* WT ($n = 5$) versus TK-*Ccrl2* KO ($n = 5$) by Student *t* test. Data from one representative out of two independent experiments are shown and expressed as mean ± SEM. **C,** Evaluation of the NK chemotactic factors CXCL10, CX3CL1, CCL5, and chemerin mRNA levels by qPCR from lung tissue. *, $P < 0.05$, TK-*Ccrl2* WT ($n = 6$) versus TK-*Ccrl2* KO ($n = 6$) by Student *t* test. Data from one representative out of two independent experiments are shown and expressed as mean ± SEM.

evaluated in lung of TK-C*crl2*–deficient and WT mice. TK-*Ccrl2*–deficient mice had a marked reduction of *Cxcl10*, *Cx3cl1*, *Ccl5*, and *Rarres2* (chemerin) mRNA expression compared with WT animals (Fig. 3C). Of note, these chemotactic factors were expressed in a similar manner in the lung of naïve TK-*Ccrl2*–deficient and TK-*Ccrl2* WT mice. Tumor growth caused a significant reduction of *Ccl5*, *Cx3cl1*, and *Rarres2* mRNA expression in both mouse strains; however, the reduction was more marked in TK-*Ccrl2*–deficient compared with WT mice (Fig. 3C). Third, the lung expression of three cytokines known to have a crucial role in NK-cell differentiation, activation, survival, and in maintaining peripheral cell homeostasis, namely IL2, IL15, and IL18 (29) was evaluated. qPCR performed with lung extracts of TK-*Ccrl2*–deficient mice revealed reduced levels for both IL2 and IL15 transcripts, whereas IL15Rα chain and IL18 expression did not differ between the two mouse strains (Fig. 4A). Fourth, the

Published OnlineFirst September 4, 2019; DOI: 10.1158/2326-6066.CIR-19-0168

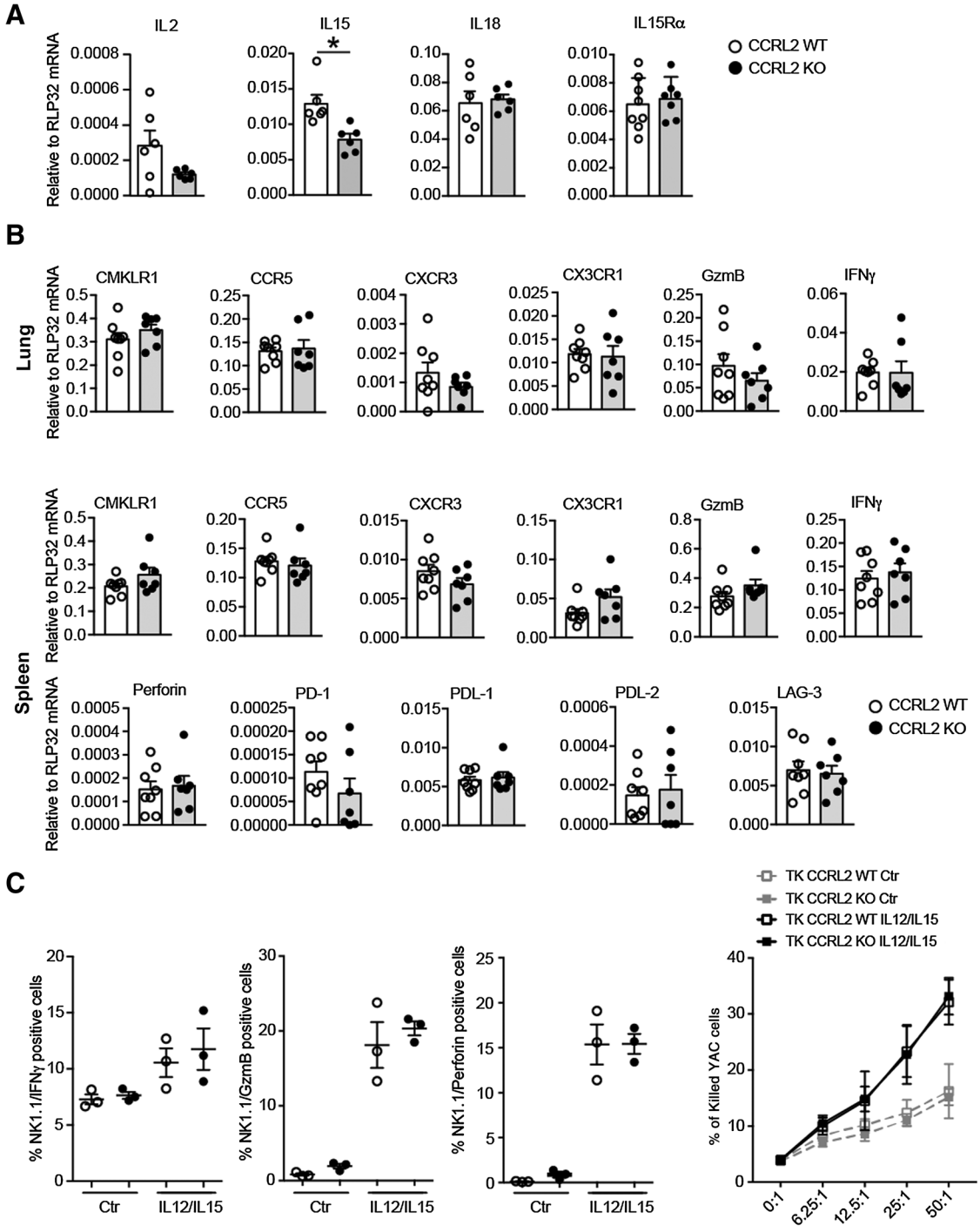

Figure 4.

Functional analysis of NK cells from TK-*Ccrl2* WT and TK-*Ccrl2* KO mice 10 weeks after Ad5CMVCre infection. **A,** qPCR for IL2, IL15, and IL18 from lung extracts (TK-*Ccrl2* WT $n = 6$, TK-*Ccrl2* KO $n = 6$) and for IL15Rα chain from sorted lung NK cells (TK-*Ccrl2* WT $n = 8$, TK-*Ccrl2* KO $n = 7$). Significance was determined by a Student *t* test, *, $P < 0.05$. Data from one representative out of two independent experiments are shown and expressed as mean ± SEM. **B,** qPCR for chemokine and chemokine receptors, effector proteins, and immune checkpoint molecules in lung and splenic sorted NK cells. TK-*Ccrl2* WT $n = 8$, TK-*Ccrl2* KO $n = 7$, by Student *t* test. Data from one representative out of two independent experiments are shown and expressed as mean ± SEM. GzmB, Granzyme B. **C,** Percentage of IFNγ$^+$, Granzyme B$^+$, and Perforin$^+$ in CD3$^-$NK1.1$^+$ splenocytes after overnight culture with medium (Ctr) or with IL12 and IL15 by FACS analysis (left), TK-*Ccrl2* WT $n = 3$, TK-*Ccrl2* KO $n = 3$, by Student *t* test. GzmB, Granzyme B. Cytotoxic activity of unstimulated (Ctr) or IL12/15-stimulated splenocytes (E) against YAC-1 target cells (T) at E/T ratios ranging from 1/1 to 50/1 by FACS analysis (right). TK-*Ccrl2* WT Ctr and TK-*Ccrl2* KO Ctr $n = 5$, TK-*Ccrl2* WT IL12/IL15 and TK-*Ccrl2* KO IL12/IL15 $n = 7$, by Student *t* test. Data from one representative out of two independent experiments are shown and expressed as mean ± SEM.

Published OnlineFirst September 4, 2019; DOI: 10.1158/2326-6066.CIR-19-0168

expression of some of the key transcription factors involved in NK-cell maturation and mobilization from bone marrow (e.g., AIOLOS, E4BP4, EOMES and Tbet; ref. 30) or in IL15 responsiveness (i.e., ID2; ref. 31) was investigated. NK cells purified from lung and spleen of tumor-bearing mice displayed no gross differences in the expression of the aforementioned transcription factors between the two mouse strains (Supplementary Fig. S3). Taken together, these results provided molecular evidence for the altered distribution of NK-cell subsets in *Ccrl2*-deficient mice and suggested that CCRL2 is involved in NK-cell tissue distribution rather than the regulation of NK-cell maturation.

To investigate the role of NK cells in *Kras/Tp53*–induced lung cancer, NK cells were depleted in TK-*Ccrl2* WT mice. The administration of an anti-NK1.1 mAb during tumor progression significantly increased the number of tumor lesions, recapitulating the phenotype of TK-*Ccrl2*–deficient mice (Supplementary Fig. S4A; $P < 0.01$). As expected, anti-NK1.1 treatment efficiently depleted NK cells in the lung, spleen, and blood compartments (Supplementary Fig. S4B). Taken together, these results demonstrate that CCRL2 controls the recruitment of NK cells and the growth of *Kras/Tp*53–driven lung tumors in a CCRL2-mediated manner.

Of note, NK cells from TK-*Ccrl2* WT naïve or tumor-bearing mice did not express membrane CCRL2 at the time of purification or after overnight stimulation with the activating cytokines IL12 and IL15 (Supplementary Fig. S4C). In addition, *Ccrl2* deficiency did not affect NK-cell membrane phenotype and function, such as the expression of chemotactic receptors (e.g., CMKLR1, CXCR3, CX3CR1, and CCR5), effector proteins (i.e., IFNγ, Granzyme B and Perforin), immune checkpoint molecules (i.e., PD-1, PDL-1, PDL-2, and LAG3), nor cytotoxic activity, as evaluated in sorted NK cells from lung and spleen (Fig. 4B and C).

Ccrl2 deficiency promoted the orthotopic growth of LG1233 cells

The role of CCRL2 in tumor progression was further investigated by the intravenous administration of LG1233 cells, a cell line derived from TK mice (24, 25), into *Ccrl2*-deficient or WT mice. *Ccrl2*-deficient mice showed significant reduction of mice survival, compared with *Ccrl2* WT animals. This effect was associated with increased tumor burden, as evaluated by histologic analysis of lung sections at 13 days postinoculum (Fig. 5A and B). Also in this experimental model, *Ccrl2*-deficient mice showed a reduced frequency of lung $CD3^{-}NK1.1^{+}$ NK cells, further supporting a role for CCRL2 in NK cell–dependent immunosurveillance in lung tumor growth (Fig. 5C). Finally, the increase in tumor burden observed following *in vivo* administration of an anti-CCRL2, known to recapitulate *Ccrl2*-deficient phenotype (18), further supports the role of CCRL2 in promoting lung tumor growth in this experimental system (Fig. 5D).

The role of CCRL2-expressing nonhematopoietic cells in lung tumor growth in TK mice

Because CCRL2 is expressed both by hematopoietic and nonhematopoietic cells (12), bone marrow chimaeras were used to evaluate the possible contribution of CCRL2 expression by endothelial/epithelial cells in lung tumor growth. Injection of bone marrow obtained from TK-*Ccrl2* WT animals to lethally irradiated TK-*Ccrl2*–deficient mice did not change the number of lesions. This result suggested that CCRL2 expression by the nonhematopoietic cell compartment contributed to the increased tumor formation observed in TK-*Ccrl2*–deficient mice (Fig. 6A). Within the $CD45^{-}$ cell compartment, a fraction of $CD31^{+}$ cells ($11.2 + 1.7\%$; $n = 5$) expressed CCRL2, whereas only a negligible percentage of $Epcam^{+}/CCRL2^{+}$ cells were detectable (Fig. 6B). CCRL2 expression by endothelial cells can support endothelial transmigration of CMKLR1 positive leukocytes to inflammatory sites, with CCRL2 acting as a molecule that binds chemerin on the cell membrane making it available to CMKLR1-expressing cells (14, 15). Splenic purified NK cells migrated in response to chemerin (as determined by a transmigration assay; ref. 15), an effect blocked by the pretreatment of endothelial cells with an anti-CCRL2 (Fig. 6C). These data suggest that CCRL2 plays a crucial role in the ability of NK cells to transmigrate across endothelial monolayers. In a model of ovalbumin-induced airway inflammation, *Ccrl2* was expressed by mouse bronchial epithelium (12). Because both lung endothelial and epithelial cells can express $CD31^{+}$ in mice (32), the identity of *Ccrl2*-expressing cells was further investigated by RNAscope. The specificity of the *Ccrl2* mRNA probe was first confirmed using sections of formalin-fixed cell blocks obtained from *Ccrl2*-transfected L1.2 cells as a positive control (Supplementary Fig. S5A). Conversely, no *Ccrl2* mRNA signal could be detected in sections of formalin-fixed cell blocks prepared with L1.2 mock cells (Supplementary Fig. S5B). A completely negative signal was also obtained using lung sections from *Ccrl2*-deficient mice (Supplementary Fig. S5C). In the lung sections of WT mice, *Ccrl2* mRNA was detected as a diffuse signal in the alveolar wall and in endothelial cells of large vessels (Fig. 6D, parts i and ii). The larger fraction of alveolar cells was composed of $CD31^{+}$ endothelial cells and by a minor fraction by $cytokeratin^{+}$ pneumocytes (Fig. 6D, parts iii and iv). The combination of distribution, morphology, and the lack of costaining of RNAscope slides with an anti-cytokeratin (Fig. 6D, part v) allowed us to identify *Ccrl2*-expressing cells as endothelial cells. Interestingly, CCRL2 expression by peritumoral endothelial cells was also observed by IHC in human LUAD biopsies (Fig. 6D, part vi).

CCRL2 expression in primary human LUAD correlated with improved survival

To gain insights into the clinical significance of our observations, *CCRL2* gene expression was assessed in primary human LUAD TGCA/GDC datasets. *CCRL2* expression was significantly decreased in LUAD tumors compared with paired-normal samples ($n = 57$; fold change normal vs. tumor 3.22, $P < 0.001$; Fig. 7A). However, no statistically relevant difference in *CCRL2* expression could be associated to tumor clinical stages (Fig. 7B). *CCRL2* expression was then evaluated as a possible prognostic biomarker. High and low *CCRL2*–expressing groups were defined using the optimal threshold separating *CCRL2* expression between normal versus tumor samples, with high *CCRL2*–expressing tumor samples corresponding to the expression levels present in normal tissues. Within a cohort of LUAD patients, a higher *CCRL2* expression correlated with a better clinical outcome, especially at early observational times (Fig. 7C). Taken together, these results suggested a role for CCRL2 in tuning immunosurveillance during the early phase of tumor development.

Discussion

This study reported that CCRL2 plays a nonredundant role in immunosurveillance, with a protective role in lung carcinogenesis.

Published OnlineFirst September 4, 2019; DOI: 10.1158/2326-6066.CIR-19-0168

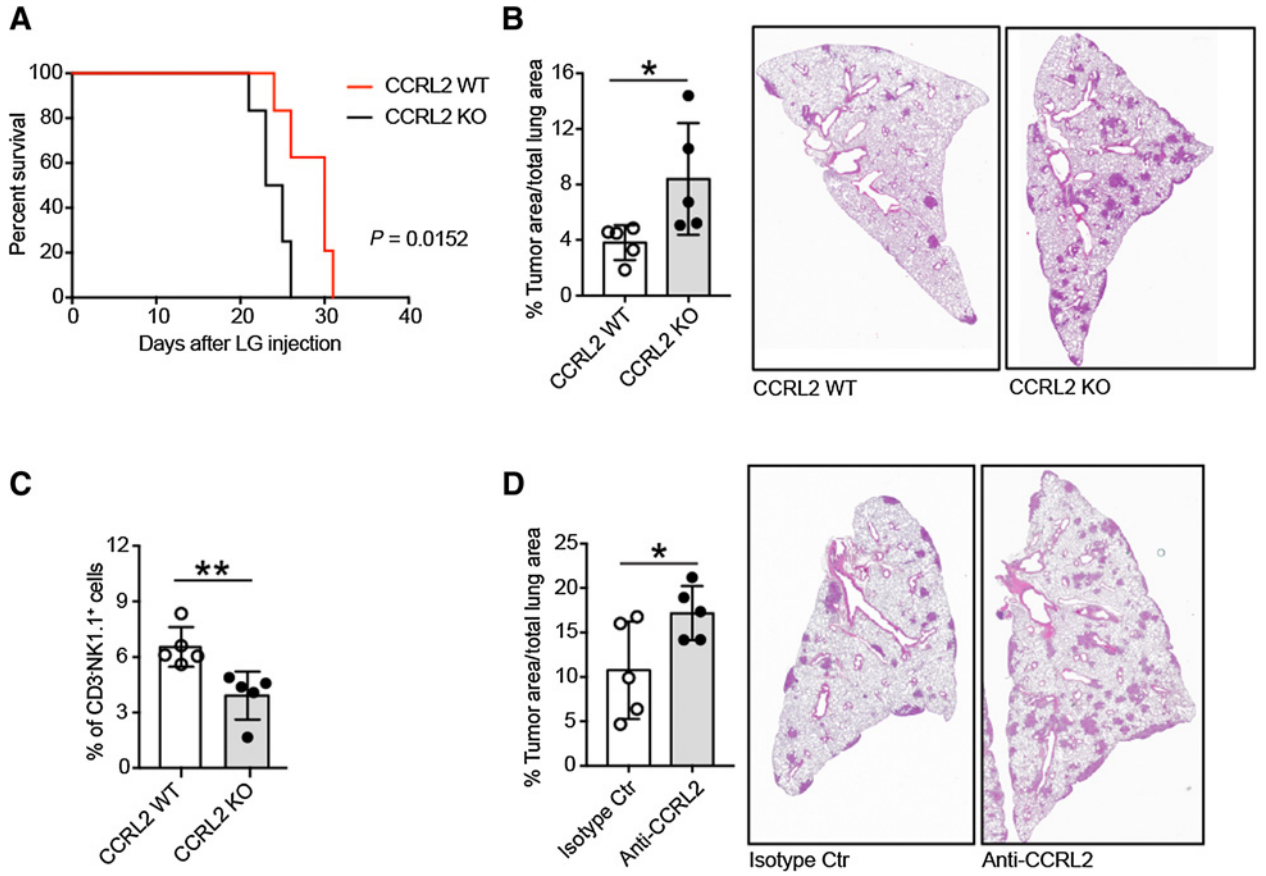

Figure 5.

Ccrl2 deficiency enhanced orthotopic growth of *Kras*-mutant LG1233 cell line. **A,** The percentage survival of *Ccrl2* WT and *Ccrl2* KO mice injected intravenously with 10^5 LG1233 cells. $P = 0.0152$, *Ccrl2* WT versus *Ccrl2* KO. **B,** Left, percentage of area occupied by tumor lesions on total lung area of *Ccrl2* WT versus *Ccrl2* KO mice sacrificed 13 days after tumor injection. *, $P < 0.05$, *Ccrl2* WT ($n = 5$) versus *Ccrl2* KO ($n = 5$) by Student *t* test. Data from one representative out of three independent experiments are shown and expressed as mean ± SEM. Right, representative images of H&E staining of *Ccrl2* WT and *Ccrl2* KO lungs. Objective magnification, ×10. **C,** FACS analysis of $CD3^-NK1.1^+$ in the $CD45^+$ population from mechanically and enzymatically treated *Ccrl2* WT and *Ccrl2* KO lungs. **, $P < 0.01$, *Ccrl2* WT ($n = 5$) versus *Ccrl2* KO ($n = 5$) by Student *t* test. Data from one representative out of three independent experiments are shown and expressed as mean ± SEM. **D,** The effect of anti-*Ccrl2* or isotype control mAb on *Ccrl2* WT mice. Appropriate antibody (100 μg/mL) was given intraperitoneally 1 day before LG1233 injection and then three times a week for the entire experiment. Left, percentage of area occupied by tumor lesions on total lung area 13 days after tumor injection; right, representative H&E images. Objective magnification, ×10. *, $P < 0.05$, anti-CCRL2 mAb ($n = 5$) versus isotype control mAb ($n = 5$) by Student *t* test. Data from one representative out of two independent experiments are shown and expressed as mean ± SEM.

This conclusion was based on the use of multiple experimental approaches, including chemically induced carcinogenesis, genetic, and transplantable models of lung cancer. The role of CCRL2 was investigated using a genetic model and a blocking anti-CCRL2. Finally, the initial analysis of TGCA/GDC datasets including 600 patients suggests a correlation between *Ccrl2* expression and LUAD patient survival.

Here, we reported a role for CCRL2 in the recruitment of innate immune cells to lung tumors. This effect included both phagocytic cells, such as monocytes, macrophages and neutrophils, and NK cells. NK cells are part of the complex network of the innate lymphoid cells and are the only known components of this family endowed with cytotoxic activity and known to express CMKLR1, the functional chemerin receptor (33, 34). A defect of cytotoxic activity of human circulating NK is correlated with increased cancer risk (33, 35–37) and growing evidence proposes a role for NK cells in the control of hematologic malignancies (38). Conversely, the ability of NK cells to control solid tumor progression has only recently becoming recognized (39–41). The current work provided evidence for the role of CCRL2 in the regulation of NK-cell distribution in lung cancer.

CCRL2 is a nonsignaling receptor for chemerin, the ligand of the chemotactic receptor CMKLR1 (16, 42). CMKLR1 is expressed by several leukocyte subsets, including NK cells (43, 44). GPR1, a third chemerin receptor is reported to be expressed in the central nervous system, skin, and adipose tissue, but the exact biological role of this receptor is still unclear (43). Although CCRL2 was not expressed by mouse NK cells, the results here presented highlight the importance of CCRL2 for the localization of NK cells to the lung. Indeed, a reduced infiltration of NK cells was observed in mice genetically deficient for CCRL2 or following the *in vivo* administration of a blocking anti-CCRL2. Of note, in both these experimental conditions and in mice administrated with an anti-NK1.1, the reduction of NK cells always correlated with increased growth of lung tumors. *In vitro*, chemerin promoted $CMKLR1^+$ NK-cell migration across a CCRL2-expressing mouse endothelial

Published OnlineFirst September 4, 2019; DOI: 10.1158/2326-6066.CIR-19-0168

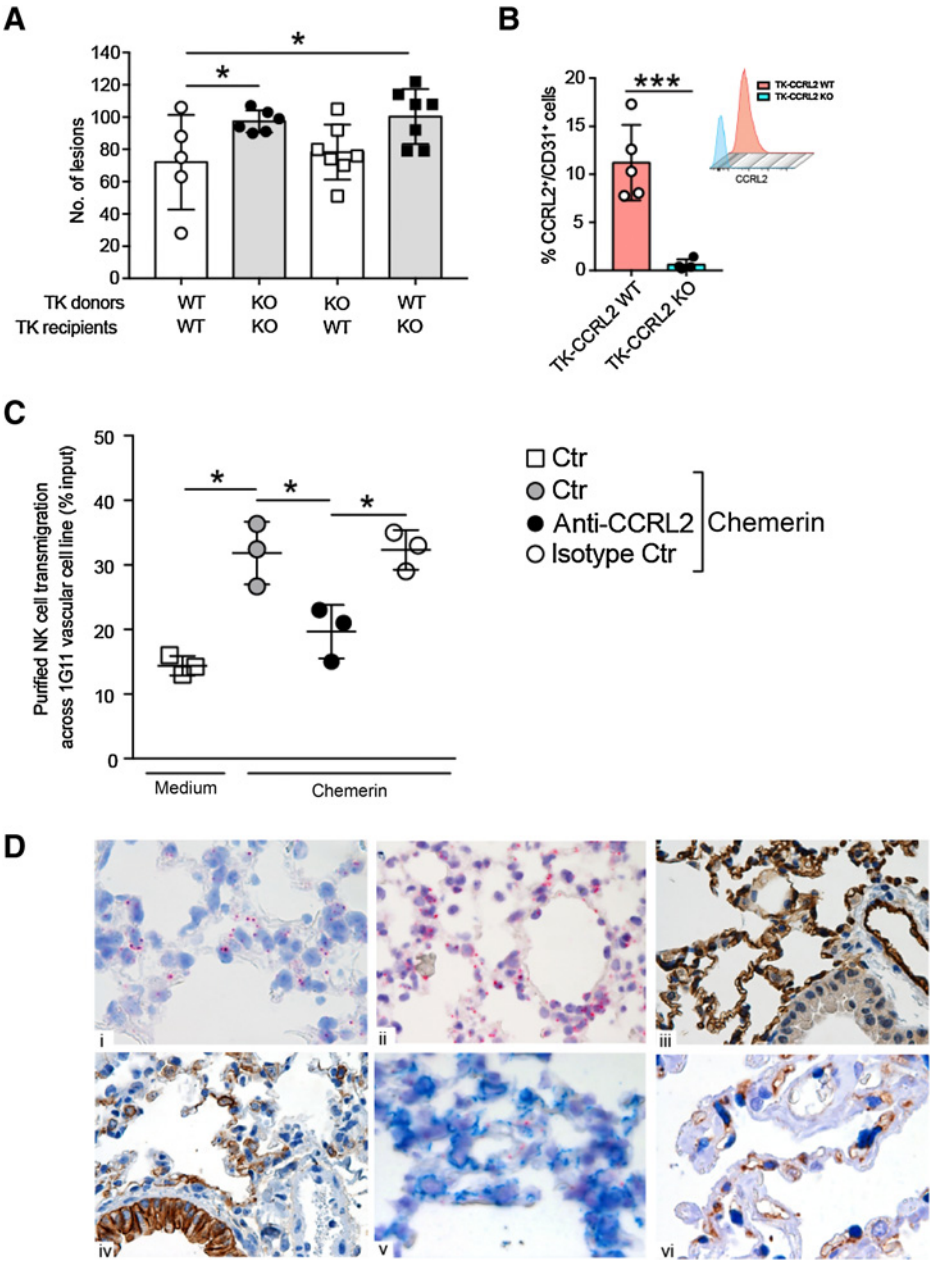

Figure 6.

CCRL2 expressed by nonhematopoietic cells played a role in the control of tumor growth. **A,** TK-*Ccrl2* WT and TK-*Ccrl2* KO mice were lethally irradiated, and then reconstituted with total bone marrow cells from TK-*Ccrl2* WT and TK-*Ccrl2* KO donor mice. Eight weeks after reconstitution, tumor development was induced by intranasal inoculation with 2.5×10^7 infectious particles of Ad5CMVCre recombinase, and then mice were sacrificed after 10 weeks. The number of lesions is indicated. *, $P < 0.05$, by generalized linear mixed model in family Poisson (TK-*Ccrl2* WT recipients of TK-*Ccrl2* WT donors, $n = 5$; TK-*Ccrl2* KO recipients of TK-*Ccrl2* KO donors, $n = 6$; TK-*Ccrl2* WT recipients of TK-*Ccrl2* KO, $n = 7$; TK-*Ccrl2* KO recipients of TK-*Ccrl2* WT donors, $n = 7$). Data from one representative out of two independent experiments are shown and expressed as mean ± SEM. **B,** CCRL2 expression on $CD31^+$ in $CD45^-$ gated cells of lungs from tumor-bearing mice and representative histograms. ***, $P < 0.001$, TK-*Ccrl2* WT ($n = 5$) versus TK-*Ccrl2* KO ($n = 4$) by Student *t* test. Data from one representative out of three independent experiments are shown and expressed as mean ± SEM. **C,** Purified splenic NK cells from *Ccrl2* WT mice were pretreated or not with anti-CCRL2 or an isotype control mAb, and their capacity to cross overnight-stimulated 1G11 vascular endothelial cells in response to chemerin (200 nmol/L) was evaluated in transmigration assay (4-hour incubation). *, $P < 0.05$, medium versus chemerin, anti-CCRL2 mAb ($n = 3$) versus chemerin, chemerin versus isotype control mAb ($n = 3$) by Student *t* test. Data from one representative out of two independent experiments are shown and expressed as mean ± SEM. **D,** *Ccrl2* mRNA expression was investigated in mouse lung by RNAscope. *Ccrl2* mRNA in alveolar wall (i), endothelial cells of a large vessel (ii), and IHC for CD31 (iii) and cytokeratin (iv) staining of *Ccrl2* WT lung. *Ccrl2* mRNA costained with anti-cytokeratin antibody (v) and double IHC of human LUAD biopsy with anti-CCRL2 and anti-ERG in the peritumoral area (vi).

Published OnlineFirst September 4, 2019; DOI: 10.1158/2326-6066.CIR-19-0168

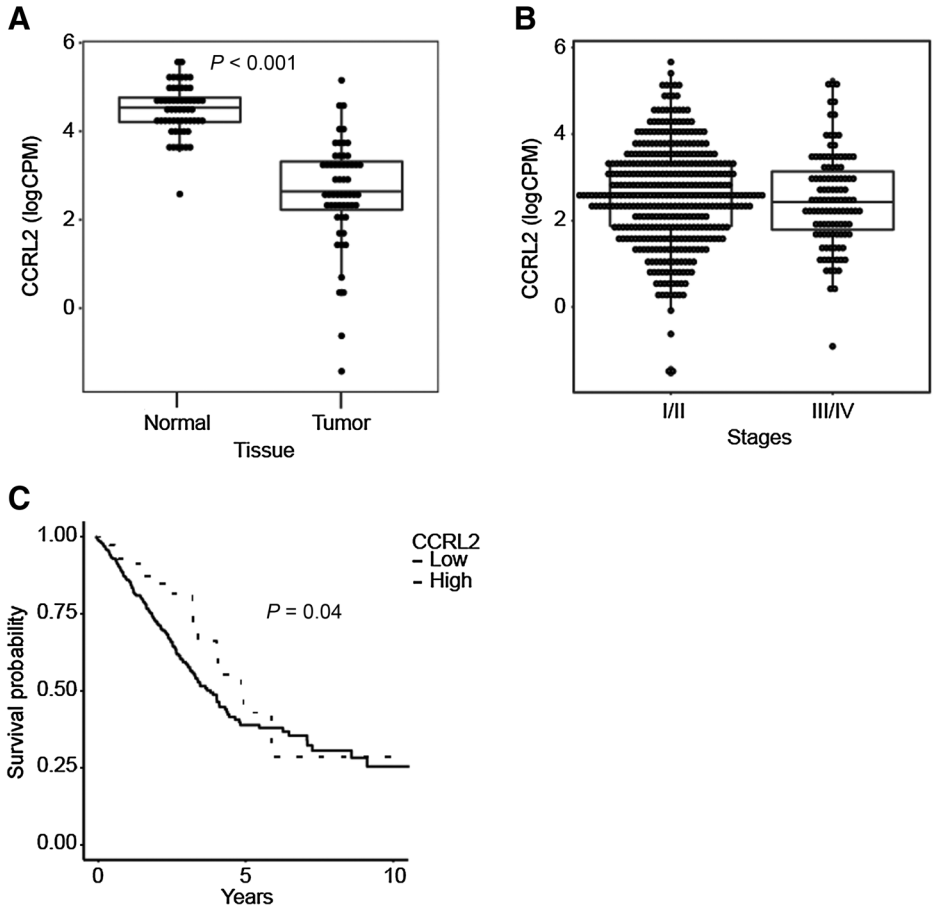

Figure 7.
CCRL2 expression in primary human LUAD correlated with improved patient survival. **A,** Boxplot showing the distribution of *CCRL2* expression values, reported as counts per million on $\log_2$ scale, both for tumor and matched normal tissues ($P < 0.001$, $n = 57$). **B,** Boxplot showing *CCRL2* expression values for tumor samples grouped by tumor stage ($n = 395$ stage I/II vs. $n = 110$ stage III/IV). **C,** Kaplan–Meier curves for overall survival for high and low *CCRL2* expression. The high-expression group was defined as those samples with *CCRL2* expression exceeding the optimal threshold separating normal from tumor samples. High expression can be considered as having a normal-like expression level (log-rank test, $P = 0.04$, $n = 424$ high vs. $n = 76$ low). Statistical significance was determined using the Mann–Whitney test. CPM, counts per million.

cell monolayer and this effect was CCRL2-dependent. This latter result extends previous observations obtained by our group and others in different experimental settings (14, 15). *Ccrl2* expression was detected in mouse lung microendothelial cells by RNAscope and by IHC in human samples of LUAD. Taking together, these results strongly suggest that CCRL2 represents an important mechanism for the recruitment of NK cells into tissue, acting as a chemerin presenting molecule at the level of endothelial cell lining microvessels. This finding is consistent with a previously proposed function of chemerin in the recruitment of NK cells in a model of artificial tumor metastasis (45) and with evidence supporting the role for endothelial cells in lung cancer (46).

The defect of NK-cell recruitment was not limited to the lung but could be detected in spleen and blood. Conversely, no change in the total number of bone marrow NK cells was observed. This result may have been the consequence of two different mechanisms. First, in TK-*Ccrl2*–deficient mice, tissue-infiltrating NK cells had altered expansion/survival properties. In this context, the expression of IL2 and IL15 was reduced in the lung of TK-*Ccrl2*–deficient mice. Both cytokines are known for their effect in peripheral NK-cell homeostasis (29). On the other hand, the expression of IL18, a cytokine involved in NK-cell activation, was unchanged. Lung macrophages and neutrophils are reported to be the responsible for IL15 production (47) as well as many proinflammatory mediators, including chemokines (48). In this study, we showed that both cell populations were reduced in lung TK-*Ccrl2*–deficient mice. Therefore, it was likely that the defect in tissue-infiltrating myeloid cells contributed to the reduced levels of tissue-infiltrating NK cells. Although this study puts the emphasis on the role of NK cells, the contribution of other cell types, such as myeloid cells, in the exacerbated tumor phenotype observed in *Ccrl2*-deficient mice, deserves further investigation.

Maturation of NK cells occurs in four different stages, according to the membrane expression of CD27 and CD11b (27). NK cell subsets express different repertoires of chemotactic receptors that regulate their chemotactic response, with the most immature subset ($CD27^+CD11b^-$) expressing CXCR4, CCR5, and CXCR3, and the most mature one ($CD27^-CD11b^+$) expressing mainly CX3CR1, CMKLR1, and S1P5 (28). In this study, we reported that $CD27^-CD11b^+$ NK cells had a reduced ability to migrate to CX3CL1 and chemerin, *in vitro*. We have previously reported that CCRL2 expression regulates the function of other chemokine receptors (i.e., CXCR2) in neutrophils, through the formation of heterodimers (18). At the moment, the ability of CCRL2 to form heterodimers with other chemotactic receptors, such as CX3CR1 or S1P5, is unknown; this might represent an additional mechanism for CCRL2 to regulate the migration of mature NK cells. The fact that some chemotactic factors relevant for NK-cell migration, such as CXCL10, CX3CL1, CCL5, and chemerin, were expressed at reduced levels in lung of TK-*Ccrl2*–deficient mice may represent a further mechanism involved in the defective recruitment of NK cells.

The finding that bone marrow was the only cell compartment investigated with a normal population of NK cells opens up the

possibility that CCRL2 might have a role in NK-cell bone marrow retention. Bone marrow medullary arteries express CCRL2 (49). Although we have not directly investigated this aspect, the fact that we did not observe changes in any other bone marrow leukocyte subset investigated argues against this possibility. Further studies are required to properly address this issue.

In our experimental conditions, CCRL2 was not expressed by lung tumor cells; however, other studies have reported CCRL2 expression by cancer cells, such as in multiple myeloma, prostate and breast carcinomas, liver metastasis, glioblastoma, and salivary adenoid cystic carcinoma (50–53). In these tumors, CCRL2 is either a tumor suppressor, such as in breast cancer (53), or a tumor promoter, such as in glioblastoma (52), suggesting that CCRL2 might have different roles in different cellular contexts. The exact function of CCRL2 expression in these tumors still needs to be elucidated.

TGCA/GDC data expression analysis in human primary LUAD showed correlation of *CCRL2* expression with clinical outcome, with higher expression levels having a protective role. In light of this result, it is tempting to speculate that CCRL2-dependent recruitment of NK cells might have a role in limiting tumor growth also in human lung cancer. A protective role of NK cells was previously described in colorectal, gastric, renal, prostate, and hepatic human tumors (39, 40, 54) and NK cells are emerging as important targets in checkpoint blockade therapies (41, 55). Therefore, our results suggest that *CCRL2* expression might represent a potential prognostic marker in patients with LUAD and a key molecule for directing NK-cell localization to the tumor site also in humans. Whether this crucial role of CCRL2 is restricted to the lung compartment or represents a general function also present in other tissues requires further investigation.

Disclosure of Potential Conflicts of Interest

A. Mantovani reports receiving a commercial research grant from Novartis, has served as a consultant/advisory board member for Novartis, Roche, Ventana, Pierre Fabre, Verily, AbbVie, Compugen, Macrophage Therapeutics, AstraZeneca, Biovelocita, BG Fund, Third Rock, and Verseau, is an inventor of patents related to PTX3 and other innate immunity molecules, and reports receiving royalties for reagents related to innate immunity. No potential conflicts of interest were disclosed by the other authors.

Authors' Contributions

Conception and design: A. Del Prete, A. Vecchi, S. Sozzani
Development of methodology: A. Del Prete, F. Sozio, T. Schioppa, V. Salvi
Acquisition of data (provided animals, acquired and managed patients, provided facilities, etc.): A. Del Prete, F. Sozio, T. Schioppa, A. Ponzetta, W. Vermi, M. Bugatti, V. Salvi, B. Bottazzi
Analysis and interpretation of data (e.g., statistical analysis, biostatistics, computational analysis): A. Del Prete, F. Sozio, T. Schioppa, A. Ponzetta, W. Vermi, S. Calza, M. Bugatti, V. Salvi, A. Vecchi, S. Sozzani
Writing, review, and/or revision of the manuscript: A. Del Prete, G. Bernardini, B. Bottazzi, A. Mantovani, S. Sozzani
Administrative, technical, or material support (i.e., reporting or organizing data, constructing databases): A. Del Prete, F. Benvenuti
Study supervision: A. Del Prete, A. Vecchi, S. Sozzani

Acknowledgments

The authors thank Dr. Patrick Brennecke for helping to set up the genetic mouse model and Roberto Leone for technical assistance in the management of animal colonies. This work was supported by the Italian Association for Cancer Research (AIRC IG-2016 grant no. 721-19014, AIRC 5 × 1000 grant no. 9962, and AIRC 5 × 1000 grant no. 21147, to A. Mantovani; IG-20776, to S. Sozzani), Fondazione Berlucchi, and Interuniversity Attraction Poles (IAP) 7-40 program. The European Commission (ERC project PHII-669415; FP7 project 281608 TIMER; ESA/ITN, H2020-MSCAITN-2015-676129), Ministero dell'Istruzione, dell'Università e della Ricerca (MIUR; project FIRB RBAP11H2R9), and Italian Ministry of Health are gratefully acknowledged. V. Salvi was a recipient of a fellowship from Fondazione Italiana Ricerca sul Cancro (FIRC). T. Schioppa is a recipient of a fellowship from Fondazione Veronesi.

The costs of publication of this article were defrayed in part by the payment of page charges. This article must therefore be hereby marked *advertisement* in accordance with 18 U.S.C. Section 1734 solely to indicate this fact.

Received April 1, 2019; revised June 25, 2019; accepted August 28, 2019; published first September 4, 2019.

References

1. Siegel RL, Miller KD, Jemal A. Cancer statistics, 2017. CA Cancer J Clin 2017;67:7–30.
2. Reck M, Rabe KF. Precision diagnosis and treatment for advanced non-small-cell lung cancer. N Engl J Med 2017;377:849–61.
3. Travis WD, Brambilla E, Riely GJ. New pathologic classification of lung cancer: relevance for clinical practice and clinical trials. J Clin Oncol 2013;31:992–1001.
4. Gridelli C, Rossi A, Carbone DP, Guarize J, Karachaliou N, Mok T, et al. Non-small-cell lung cancer. Nat Rev Dis Primers 2015;1:15009.
5. Sica A, Bronte V. Altered macrophage differentiation and immune dysfunction in tumor development. J Clin Invest 2007;117:1155–66.
6. Mantovani A, Allavena P, Sica A, Balkwill F. Cancer-related inflammation. Nature 2008;454:436–44.
7. Balkwill F. Cancer and the chemokine network. Nat Rev Cancer 2004;4:540–50.
8. Del Prete A, Schioppa T, Tiberio L, Stabile H, Sozzani S. Leukocyte trafficking in tumor microenvironment. Curr Opin Pharmacol 2017;35:40–7.
9. Bachelerie F, Ben-Baruch A, Burkhardt AM, Combadiere C, Farber JM, Graham GJ, et al. International Union of Basic and Clinical Pharmacology. [corrected]. LXXXIX. Update on the extended family of chemokine receptors and introducing a new nomenclature for atypical chemokine receptors. Pharmacol Rev 2014;66:1–79.
10. Bachelerie F, Graham GJ, Locati M, Mantovani A, Murphy PM, Nibbs R, et al. New nomenclature for atypical chemokine receptors. Nat Immunol 2014;15:207–8.
11. Massara M, Bonavita O, Mantovani A, Locati M, Bonecchi R. Atypical chemokine receptors in cancer: friends or foes? J Leukoc Biol 2016;99:927–33.
12. Del Prete A, Bonecchi R, Vecchi A, Mantovani A, Sozzani S. CCRL2, a fringe member of the atypical chemoattractant receptor family. Eur J Immunol 2013;43:1418–22.
13. Yoshimura T, Oppenheim JJ. Chemokine-like receptor 1 (CMKLR1) and chemokine (C-C motif) receptor-like 2 (CCRL2); two multifunctional receptors with unusual properties. Exp Cell Res 2011;317:674–84.
14. Monnier J, Lewen S, O'Hara E, Huang K, Tu H, Butcher EC, et al. Expression, regulation, and function of atypical chemerin receptor CCRL2 on endothelial cells. J Immunol 2012;189:956–67.
15. Gonzalvo-Feo S, Del Prete A, Pruenster M, Salvi V, Wang L, Sironi M, et al. Endothelial cell-derived chemerin promotes dendritic cell transmigration. J Immunol 2014;192:2366–73.
16. Zabel BA, Nakae S, Zuniga L, Kim JY, Ohyama T, Alt C, et al. Mast cell-expressed orphan receptor CCRL2 binds chemerin and is required for optimal induction of IgE-mediated passive cutaneous anaphylaxis. J Exp Med 2008;205:2207–20.
17. Mazzon C, Zanotti L, Wang L, Del Prete A, Fontana E, Salvi V, et al. CCRL2 regulates M1/M2 polarization during EAE recovery phase. J Leukoc Biol 2016;99:1027–33.
18. Del Prete A, Martinez-Munoz L, Mazzon C, Toffali L, Sozio F, Za L, et al. The atypical receptor CCRL2 is required for CXCR2-dependent neutrophil recruitment and tissue damage. Blood 2017;130:1223–34.

Published OnlineFirst September 4, 2019; DOI: 10.1158/2326-6066.CIR-19-0168

19. Otero K, Vecchi A, Hirsch E, Kearley J, Vermi W, Del Prete A, et al. Nonredundant role of CCRL2 in lung dendritic cell trafficking. Blood 2010;116:2942–9.
20. De Henau O, Degroot GN, Imbault V, Robert V, De Poorter C, McHeik S, et al. Signaling properties of chemerin receptors CMKLR1, GPR1 and CCRL2. PLoS One 2016;11:e0164179.
21. Mazzotti C, Gagliostro V, Bosisio D, Del Prete A, Tiberio L, Thelen M, et al. The atypical receptor CCRL2 (C-C Chemokine Receptor-Like 2) does not act as a decoy receptor in endothelial cells. Front Immunol 2017;8:1233.
22. Miller YE, Dwyer-Nield LD, Keith RL, Le M, Franklin WA, Malkinson AM. Induction of a high incidence of lung tumors in C57BL/6 mice with multiple ethyl carbamate injections. Cancer Lett 2003;198:139–44.
23. DuPage M, Dooley AL, Jacks T. Conditional mouse lung cancer models using adenoviral or lentiviral delivery of Cre recombinase. Nat Protoc 2009;4:1064–72.
24. Dimitrova N, Gocheva V, Bhutkar A, Resnick R, Jong RM, Miller KM, et al. Stromal expression of miR-143/145 promotes neoangiogenesis in lung cancer development. Cancer Discov 2016;6:188–201.
25. Caronni N, Simoncello F, Stafetta F, Guarnaccia C, Ruiz-Moreno JS, Opitz B, et al. Downregulation of membrane trafficking proteins and lactate conditioning determine loss of dendritic cell function in lung cancer. Cancer Res 2018;78:1685–99.
26. Eruslanov EB, Bhojnagarwala PS, Quatromoni JG, Stephen TL, Ranganathan A, Deshpande C, et al. Tumor-associated neutrophils stimulate T cell responses in early-stage human lung cancer. J Clin Invest 2014;124:5466–80.
27. Chiossone L, Chaix J, Fuseri N, Roth C, Vivier E, Walzer T. Maturation of mouse NK cells is a 4-stage developmental program. Blood 2009;113:5488–96.
28. Walzer T, Vivier E. G-protein-coupled receptors in control of natural killer cell migration. Trends Immunol 2011;32:486–92.
29. Di Santo JP. Natural killer cell developmental pathways: a question of balance. Annu Rev Immunol 2006;24:257–86.
30. Holmes ML, Huntington ND, Thong RP, Brady J, Hayakawa Y, Andoniou CE, et al. Peripheral natural killer cell maturation depends on the transcription factor Aiolos. EMBO J 2014;33:2721–34.
31. Delconte RB, Shi W, Sathe P, Ushiki T, Seillet C, Minnich M, et al. The helix-loop-helix protein ID2 governs NK cell fate by tuning their sensitivity to interleukin-15. Immunity 2016;44:103–15.
32. Bantikassegn A, Song X, Politi K. Isolation of epithelial, endothelial, and immune cells from lungs of transgenic mice with oncogene-induced lung adenocarcinomas. Am J Respir Cell Mol Biol 2015;52:409–17.
33. Waldhauer I, Steinle A. NK cells and cancer immunosurveillance. Oncogene 2008;27:5932–43.
34. Eberl G, Colonna M, Di Santo JP, McKenzie AN. Innate lymphoid cells. Innate lymphoid cells: a new paradigm in immunology. Science 2015;348:aaa6566.
35. Hayakawa Y, Smyth MJ. Innate immune recognition and suppression of tumors. Adv Cancer Res 2006;95:293–322.
36. Cerwenka A, Lanier LL. Natural killer cell memory in infection, inflammation and cancer. Nat Rev Immunol 2016;16:112–23.
37. Chiossone L, Dumas PY, Vienne M, Vivier E. Natural killer cells and other innate lymphoid cells in cancer. Nat Rev Immunol 2018;18:671–88.
38. Gismondi A, Stabile H, Nisti P, Santoni A. Effector functions of natural killer cell subsets in the control of hematological malignancies. Front Immunol 2015;6:567.
39. Malmberg KJ, Carlsten M, Bjorklund A, Sohlberg E, Bryceson YT, Ljunggren HG. Natural killer cell-mediated immunosurveillance of human cancer. Semin Immunol 2017;31:20–9.
40. Molgora M, Bonavita E, Ponzetta A, Riva F, Barbagallo M, Jaillon S, et al. IL-1R8 is a checkpoint in NK cells regulating anti-tumour and anti-viral activity. Nature 2017;551:110–4.
41. Barry KC, Hsu J, Broz ML, Cueto FJ, Binnewies M, Combes AJ, et al. A natural killer-dendritic cell axis defines checkpoint therapy-responsive tumor microenvironments. Nat Med 2018;24:1178–91.
42. Wittamer V, Franssen JD, Vulcano M, Mirjolet JF, Le Poul E, Migeotte I, et al. Specific recruitment of antigen-presenting cells by chemerin, a novel processed ligand from human inflammatory fluids. J Exp Med 2003;198:977–85.
43. Bondue B, Wittamer V, Parmentier M. Chemerin and its receptors in leukocyte trafficking, inflammation and metabolism. Cytokine Growth Factor Rev 2011;22:331–8.
44. Sozzani S, Vermi W, Del Prete A, Facchetti F. Trafficking properties of plasmacytoid dendritic cells in health and disease. Trends Immunol 2010;31:270–7.
45. Pachynski RK, Zabel BA, Kohrt HE, Tejeda NM, Monnier J, Swanson CD, et al. The chemoattractant chemerin suppresses melanoma by recruiting natural killer cell antitumor defenses. J Exp Med 2012;209:1427–35.
46. Kim WY, Perera S, Zhou B, Carretero J, Yeh JJ, Heathcote SA, et al. HIF2alpha cooperates with RAS to promote lung tumorigenesis in mice. J Clin Invest 2009;119:2160–70.
47. Muro S, Taha R, Tsicopoulos A, Olivenstein R, Tonnel AB, Christodoulopoulos P, et al. Expression of IL-15 in inflammatory pulmonary diseases. J Allergy Clin Immunol 2001;108:970–5.
48. Castriconi R, Carrega P, Dondero A, Bellora F, Casu B, Regis S, et al. Molecular mechanisms directing migration and retention of natural killer cells in human tissues. Front Immunol 2018;9:2324.
49. Tikhonova AN, Dolgalev I, Hu H, Sivaraj KK, Hoxha E, Cuesta-Dominguez A, et al. The bone marrow microenvironment at single-cell resolution. Nature 2019;569:222–8.
50. Reyes N, Benedetti I, Rebollo J, Correa O, Geliebter J. Atypical chemokine receptor CCRL2 is overexpressed in prostate cancer cells. J Biomed Res 2019;33:17–23.
51. Akram IG, Georges R, Hielscher T, Adwan H, Berger MR. The chemokines CCR1 and CCRL2 have a role in colorectal cancer liver metastasis. Tumour Biol 2016;37:2461–71.
52. Yin F, Xu Z, Wang Z, Yao H, Shen Z, Yu F, et al. Elevated chemokine CC-motif receptor-like 2 (CCRL2) promotes cell migration and invasion in glioblastoma. Biochem Biophys Res Commun 2012;429:168–72.
53. Wang LP, Cao J, Zhang J, Wang BY, Hu XC, Shao ZM, et al. The human chemokine receptor CCRL2 suppresses chemotaxis and invasion by blocking CCL2-induced phosphorylation of p38 MAPK in human breast cancer cells. Med Oncol 2015;32:254.
54. Pasero C, Gravis G, Granjeaud S, Guerin M, Thomassin-Piana J, Rocchi P, et al. Highly effective NK cells are associated with good prognosis in patients with metastatic prostate cancer. Oncotarget 2015;6:14360–73.
55. Hsu J, Hodgins JJ, Marathe M, Nicolai CJ, Bourgeois-Daigneault MC, Trevino TN, et al. Contribution of NK cells to immunotherapy mediated by PD-1/PD-L1 blockade. J Clin Invest 2018;128:4654–68.

AACR American Association for Cancer Research

Cancer Immunology Research

The Atypical Receptor CCRL2 Is Essential for Lung Cancer Immune Surveillance

Annalisa Del Prete, Francesca Sozio, Tiziana Schioppa, et al.

Cancer Immunol Res Published OnlineFirst September 4, 2019.